Twist-Induced Near-Field Radiative Heat Switch in Hyperbolic Antiferromagnets

Yuanyang Du, Jiebin Peng,[*] Zhong Shi, and Jie Ren[†]
Center for Phononics and Thermal Energy Science, China-EU Joint Lab on Nanophononics, Shanghai Key Laboratory of Special Artificial Microstructure Materials and Technology, School of Physics Science and Engineering, Tongji University, Shanghai 200092, China

We study the twist-induced control of the near-field radiative heat transfer between two hyperbolic antiferromagnetic insulators under external magnetic fields. We show that the near-field heat flux can be affected by both the twist angle θ and the magnitude of the applied magnetic field with different broken symmetries. Irrespective of the twist angle, the external magnetic field causes the radiative heat flux to change nonmonotonically, and the minimum heat flux can be found with magnetic fields of approximately 1.5 T. Such nonmonotonic behavior is because the magnetic field can radically change the nature of the magnon polaritons with time-reversal symmetry breaking. The field not only affects the topological structure of surface magnon polaritons but also induces volume magnon polaritons that progressively dominate the heat transfer as the field increases. We further propose a twist-induced thermal switch device with inversion symmetry breaking, which can strongly regulate radiative heat flux through different magnetic fields. Our findings account for a characteristic modulation of radiative heat transfer with implications for applications in efficient thermal management.

I. INTRODUCTION

Thermal radiation is one of the most common phenomena and plays a significant role in basic disciplines and technology applications. Presently, the investigation of radiative heat transfer between closely spaced objects is receiving much attention. The traditional Stefan-Boltzmann law can be broken at the nanoscale, as the coupling of evanescent waves provides extra radiation channels for heat transfer [1–4], which has been verified in various experiments exploring different materials, geometrical shapes, and gaps ranging from micrometers to a few nanometers [5]. These experiments have also triggered the hope that near-field radiative heat transfer (NFRHT) could have an impact on different technologies such as data carrier storage [6–8], coherent thermal sources [9,10], scanning thermal microscopy [11–13], active noncontact thermal management [14–16], thermophotovoltaics [17, 18], and other energy conversion devices [19].

In recent years, one of the significant research lines in the territory of radiative heat transfer has been searching for materials where NFRHT can be greatly enhanced. To date, the largest NFRHT enhancements have been reported for polar dielectrics, in which NFRHT is dominated by surface phonon polaritons [20,21]. Similar enhancements have been predicted and observed in doped semiconductors due to surface plasmon polaritons [22,23]. Subsequently, several van der Waals heterostructures can support surface phonon-plasmon polaritons, which also enhance NFRHT [24–26]. Apart from these, surface magnon polaritons (SMPs), which can be excited in magnetic media, play a significant role in NFRHT due to their striking hyperbolic behavior [27,28].

Another key issue in the territory of radiative heat transfer is the active control and modulation of NFRHT. Several strategies have been proposed, such as applying an electric field to phase-change materials [29] or ferroelectric materials [30] and applying a magnetic field to magneto-optical materials [31,32] or magnetic Weyl semimetals [33–35]. Another active control strategy utilizes the rotational degree of freedom [36,37], and similar twist-induced concepts have been demonstrated in two-dimensional materials [38,39] and photonics [40,41]. This control strategy is called the twisting method.

In this work, we present a theoretical analysis of the impact of an external magnetic field on the radiative heat transfer between two parallel plates made of an antiferromagnetic insulator (AFMI) for different twist angles. We find that the presence of a magnetic field makes the radiative heat flux change nonmonotonically, and we show that the reduction can be as large as 25% for fields of approximately 1.5 T. This phenomenon occurs because the magnetic field not only strongly modifies the width of the band where SMPs can be excited that normally dominate

───────────
[*]jiebinxonics@tongji.edu.cn
[†]xonics@tongji.edu.cn

NFRHT, but also generates nonreciprocal volume magnon polaritons (VMPs) via time-reversal symmetry breaking, which can dominate the heat transfer as the field increases. Apart from these, we utilize the nonreciprocity of VMPs to obtain a twist-induced thermal switch. To enhance the twist-induced thermal switch ratio, we actively select the heat transfer channels sensitive to twist by applying specific magnetic fields. Thus, our work offers an effective strategy to regulate NFRHT between antiferromagnets and provides an attractive recipe to design devices with height adjustable characteristics.

II. THEORETICAL FORMALISM FOR NEAR-FIELD RADIATIVE HEAT TRANSFER

As schematically depicted in Fig. 1(a), the system consists of two AFMI slabs with twist angle in the presence of a magnetic field. The structures are separated by a vacuum gap of width d and held at temperatures T_1 (T_2), where the magnetic field B_1 (B_2) is applied along the y (y') direction as the relative twist angle is expressed as θ. From fluctuational electrodynamics, the heat transfer coefficient (HTC) between two AFMI slabs for a temperature T is given by the following Landauer-like expression [1]:

$$h(T, \theta, B) = \int_0^\infty \frac{\partial \Theta(\omega, T)}{\partial T} \Phi(\omega, \theta, B) d\omega, \qquad (1)$$

where $\Theta(\omega, T) = \hbar\omega/[e^{(\hbar\omega/k_B T)} - 1]$ represents the average photon energy of Planck oscillators at an angular frequency ω and temperature T, and $\Phi(\omega, \theta, B) = \int_{-\infty}^{\infty} \int_{-\infty}^{\infty} \xi(\omega, k_x, k_y)/8\pi^3 dk_x dk_y$, where $k = \sqrt{k_x^2 + k_y^2}$ is the wave vector parallel to the surface planes and $\xi(\omega, k_x, k_y)$ with twist angle θ characterizes the energy transmission coefficient that describes the probability of photons being excited by thermal energy, which can be expressed as [36]

$$\xi = \begin{cases} \text{Tr}[(\mathbf{I} - \mathbf{R}_2^\dagger \mathbf{R}_2)\mathbf{D}(\mathbf{I} - \mathbf{R}_1\mathbf{R}_1^\dagger)\mathbf{D}^\dagger], & k < \omega/c, \\ \text{Tr}[(\mathbf{R}_2^\dagger - \mathbf{R}_2)\mathbf{D}(\mathbf{R}_1 - \mathbf{R}_1^\dagger)\mathbf{D}^\dagger]e^{-2|k_z|d}, & k > \omega/c, \end{cases} \qquad (2)$$

where $k_z = \sqrt{k_0^2 - k^2}$ represents the wave vector vertical to the surface planes in the vacuum gap and $\dagger$ signifies the complex conjugate transpose. $\mathbf{I}$ is a 2×2 unit matrix and the 2×2 matrix $\mathbf{D}$ is defined as $\mathbf{D} = (\mathbf{I} - \mathbf{R}_1\mathbf{R}_2 e^{2ik_z d})^{-1}$, which describes the Fabry-Perot-like denominator. The 2×2 matrix $\mathbf{R}_a$ is in the reflection coefficient tensor of different polarizations.

To clarify the enhancement of the heat transfer channel coupling degree and to simplify the analysis, we first consider the situation in which the external magnetic fields have the same value, i.e., $B_1 = B_2 = B_0$. In this case,

the permeability tensor of the bottom AFMI slab has the form [42]

$$\mu = \begin{bmatrix} \mu_{xx} & 0 & \mu_{xz} \\ 0 & \mu_{yy} & 0 \\ \mu_{zx} & 0 & \mu_{zz} \end{bmatrix}, \qquad (3)$$

where

$$\mu_{xx} = 1 + \frac{2\mu_0\gamma^2 M_S B_0 \sin\alpha}{\omega_\perp^2 - (\omega + i\Gamma)^2},$$
$$\mu_{yy} = 1 + \frac{2\mu_0\gamma^2 M_S B_A \cos^2 a}{\omega_\parallel^2 - (\omega + i\Gamma)^2},$$
$$\mu_{zz} = 1 + \frac{2\mu_0\gamma^2 M_S (B_0 \sin\alpha + B_A \cos 2\alpha)}{\omega_\perp^2 - (\omega + i\Gamma)^2}, \qquad (4)$$
$$\mu_{xz} = -\mu_{zx} = -i\frac{2\mu_0\gamma (M_S(\omega + i\Gamma) \sin\alpha)}{\omega_\perp^2 - (\omega + i\Gamma)^2},$$

where B_A measures the anisotropy force and B_E is the exchange force that is exerted on each ion by the ions forming the other sublattice. The sublattice magnetization M_s will point predominantly parallel and antiparallel to a preferred axis along the x direction. Then, γ and Γ are gyromagnetic ratio and damping parameters, respectively [43]. Moreover, $\omega_\parallel$ and $\omega_\perp$ are the components of the resonance parallel and perpendicular to the magnetic field and depend on the value of the magnetic field. These can be expressed as

$$\omega_\parallel^2 = \omega_0^2 \cos^2\alpha,$$
$$\omega_\perp^2 = \omega_0^2 \cos^2\alpha + 2\gamma^2 B_0 B_E \sin\alpha, \qquad (5)$$

where $\omega_0 = \gamma(2B_A B_E + B_A^2)^{1/2}$ represents the resonance frequency in the absence of a magnetic field and the spins cant at an angle $\alpha = \arcsin(B_0)/(B_A + 2B_E)$ in the x-y plane [42]. The permeability tensor of the top AFMI slab is written as $\mu' = \mathcal{R}(\theta)\mu\mathcal{R}^T(\theta)$ with the rotation matrix $\mathcal{R}(\theta)$ along the z axis.

Distinct from nonmagnetic crystals, the indefinite behavior in magnetic media can be controlled with a magnetic field, which affects the magnon polariton resonance frequency. If a magnetic field is applied to generate spin canting [see Fig. 1(c)], the main effect is to shift the resonance $\omega_\perp$ to higher frequencies. In contrast [see Fig. 1(d)], irrespective of the magnetic field, the resonance $\omega_\parallel$ is basically unchanged. Therefore, the resonance and its features, such as the condition to obtain negative refraction where $\mu_{yy}\mu_{zz} < 0$ and where $\mu_{yy} < 0$ and $\mu_{zz} < 0$, are also tuned to different frequencies [28,44]. This hyperbolic behavior plays a significant role in NFRHT.

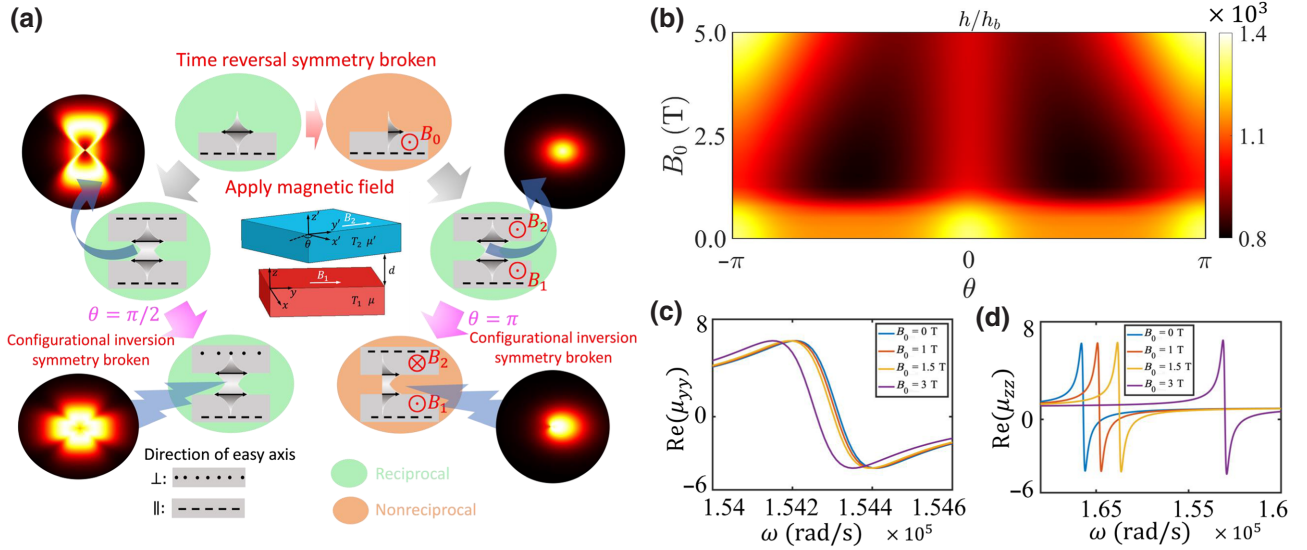During the numerical calculation, we adopt the parameters of manganese difluoride (MnF$_2$), which have been

FIG. 1. (a) Schematic of the near-field radiative heat transfer between two semi-infinite AFMIs. The thickness of vacuum gap is d. The twist angle θ is defined by the anticlockwise rotation of $x'y'z'$ coordinate system with respect to xyz coordinate system. The energy transmission coefficients for wave vector space reflect the symmetry of electromagnetic modes. Note that applying a magnetic field and twisting break the time-reversal symmetry and configuration inversion symmetry. (b) The heat transfer coefficient varying with magnetic field at different twist angle. (c) Real part of the y-direction component of permeability tensor of AFMI. (d) Real part of the z-direction component of permeability tensor of AFMI.

reported [45], anisotropy force $B_A = 0.787$ T, exchange force $B_E = 55.0$ T, sublattice magnetization $M_s = 6.0 \times 10^5$ A/m, permittivity $\varepsilon = 5.5$, and gap distance $d = 20$ nm. At a temperature of 28 K, we have the gyromagnetic ratio $\gamma/2\pi c = 0.877$ cm^{-1}/T and damping parameters $\Gamma/\omega_0 = 6.5 \times 10^{-4}$.

III. RESULTS AND DISCUSSION

A. Symmetry analysis for near-field radiative heat transfer

Before illustrating the main findings, we first give a basic symmetry analysis for MP-dominated radiative heat flux. As shown in Fig. 1(a), an applied magnetic field can cause a nonreciprocal surface electromagnetic mode on one AFMI slab due to time-reversal symmetry breaking (①→④). Regardless of the external magnetic field in ② and ⑤, the transmissions between the two AFMI slabs both have a high degree of symmetry in k_x-k_y space under the inversion symmetry protected configuration due to the mismatch between different nonreciprocal MPs. When the configurational inversion symmetry is broken from ⑤ to ⑥ (twist angle $\theta = \pi$), we can find a strong nonreciprocal effect in the transmission plot due to the strong near-field coupling between nonreciprocal MPs at such a configuration. Similar results are not found in the reciprocal-MP-dominated system under configurational symmetry breaking (③) [46]. After qualitative analysis of symmetry, Fig. 1(b) quantitatively shows that the NFRHT between

the AFMI slabs can be strongly controlled by the magnetic field and twist angle θ. Note that we consider this work at a cryogenic temperature of 28 K. In this case, the heat transfer performance of antiferromagnets is similar to that of gyroelectric materials at room temperature, which has enlightening significance for near-field radiative heat transfer at low temperatures [31]. Whether it is a magnetic responsive or an electric responsive material, the working temperature mainly depends on its resonance frequency. Primarily, the maximum value of HTC is approximately twice the minimum value, which corresponds to the light region and dark region, respectively, in the phase image. Moreover, it is obvious that the presence of a magnetic field makes the HTC change nonmonotonically, and twist operation induces the thermal switch effect. We demonstrate this in detail in the following discussions.

B. Magnetic field dependence of NFRHT

In Fig. 2(a), we show the HTC as a function of the value of the magnetic field for different twist angles. There are three salient features: (i) irrespective of the twist angle, the heat transfer decreases and then increases with increasing magnetic field, (ii) the maximum reduction of HTC up to 25% can be found with a magnetic field of approximately 1.5 T, and (iii) in the interval where the magnetic field has positive feedback to the heat transfer, the enhancement effect of heat transfer decreases with increasing twist angle; in particular, the HTC is nearly unchanged where the twist angle $\theta = 0$. The strong modification of heat
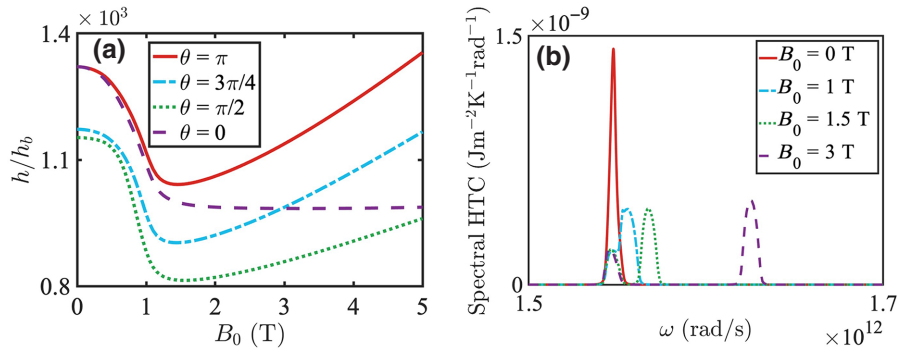
FIG. 2. (a) The heat transfer coefficient varying with magnetic field at different twist angle. (b) The heat transfer coefficient spectral function for different magnetic fields where the twist angle $\theta = \pi$.

transfer due to the magnetic field is even more apparent in the spectral HTC. As shown in Fig. 2(b), the magnetic field not only distorts and reduces the height of the peaks related to the surface waves but also generates two new peaks that eventually replace the initial peak. One of the peaks remains basically unchanged. In contrast, the other peak shifts to higher frequencies as the field increases. This additional peak appears at the resonance $\omega_\perp$ and its presence illustrates the high tunability that can be achieved.

To shed more light on these results, it is convenient to examine the transmission coefficients in different directions of the wave vector. We focus on exploring the s-polarized waves, which can be shown to dominate the heat transfer. Figures 3(a) and 3(b) present the corresponding energy transmission coefficients in ω-k space with different values of magnetic field. On the one hand, if the wave propagates along the y direction, the transmission maxima are located around a low restricted area of k and ω at a low magnetic field, indicating that surface waves dominate the NFRHT. Figure 3(a)① also shows that the magnetic field can modify the dispersion relation of magnon polaritons. By increasing the magnitude of the magnetic field, the channel of SMPs is progressively replaced by the channels of VMPs, and the surface waves are restricted to the narrow reststrahlen band for a higher magnetic field [see Fig. 3(a)②]. As shown in Fig. 3(a)③,④, at a large magnetic field, the NFRHT is dominated by the channels of VMPs. It is obvious that the transmission corresponding to the low-frequency band is little changed, and the transmission corresponding to the high-frequency band only has a frequency shift, which is dependent on the value of the magnetic field. On the other hand, considering that the wave is along the x direction, Fig. 3(b)①,④ shows that the VMPs dominate the NFRHT and that the frequency and cutoff wave vector k corresponding to the transmission maxima gradually increase with increasing magnetic field. In summary, the modes that dominate NFRHT change from SMPs into VMPs as the magnetic field increases.

To explain the nature of the magnetic-field-induced modes mentioned above, it is significant to note that the off-diagonal elements of the permeability tensor (nonreciprocal term) play little role in radiative heat transfer ($\mu_{xz} \ll \mu_{xx,yy,zz}$). Therefore, we assume that the polarization conversion is irrelevant and that the plates effectively behave as biaxial media where their permeability tensors are diagonal: $\hat{\mu} = \mathrm{diag}[\mu_{xx}, \mu_{yy}, \mu_{zz}]$. Within this approximation (biaxial approximation), it is easy to compute the dispersion relation of the SMPs: finding the singular value of the denominator of the transmission coefficient, i.e.,

$$1 - r_{ss}^2 e^{-2|k_z|d} = 0, \tag{6}$$

where the reflection coefficient $r_{ss} = (k_z \mu_{yy} - k_z')/(k_z \mu_{yy} + k_z')$ and k_z' is the z component of the wave vector in the AFMI. The cyan dashed lines in Figs. 3(a) and 3(b) show that the dispersion relation reproduces the maximum of the transmission in the frequency regions where surface waves are allowed ($\mu_{yy}, \mu_{zz} < 0$). The nature of VMPs can also be understood within the biaxial approximation. After matching the boundary conditions, the dispersion of the VMPs with different wave propagation directions can be written as follows:

$$\begin{aligned}
\frac{k_y^2}{\mu_{zz}} + \frac{k_z'^2}{\mu_{yy}} &= \epsilon \left(\frac{\omega}{c}\right)^2, \\
\frac{k_x^2}{\mu_{zz}} + \frac{k_z'^2}{\mu_{xx}} &= \epsilon \left(\frac{\omega}{c}\right)^2.
\end{aligned} \tag{7}$$

The dispersion of VMPs becomes hyperbolic when $\mu_{yy}\mu_{zz} < 0$ or $\mu_{xx}\mu_{zz} < 0$. As illustrated in Figs. 3(a)②–④ and 3(b)①–④, the hyperbolic regions correspond exactly to the areas where the transmission reaches its maximum for a broad range of k values. This fact shows that our AFMI plates effectively behave as hyperbolic materials.
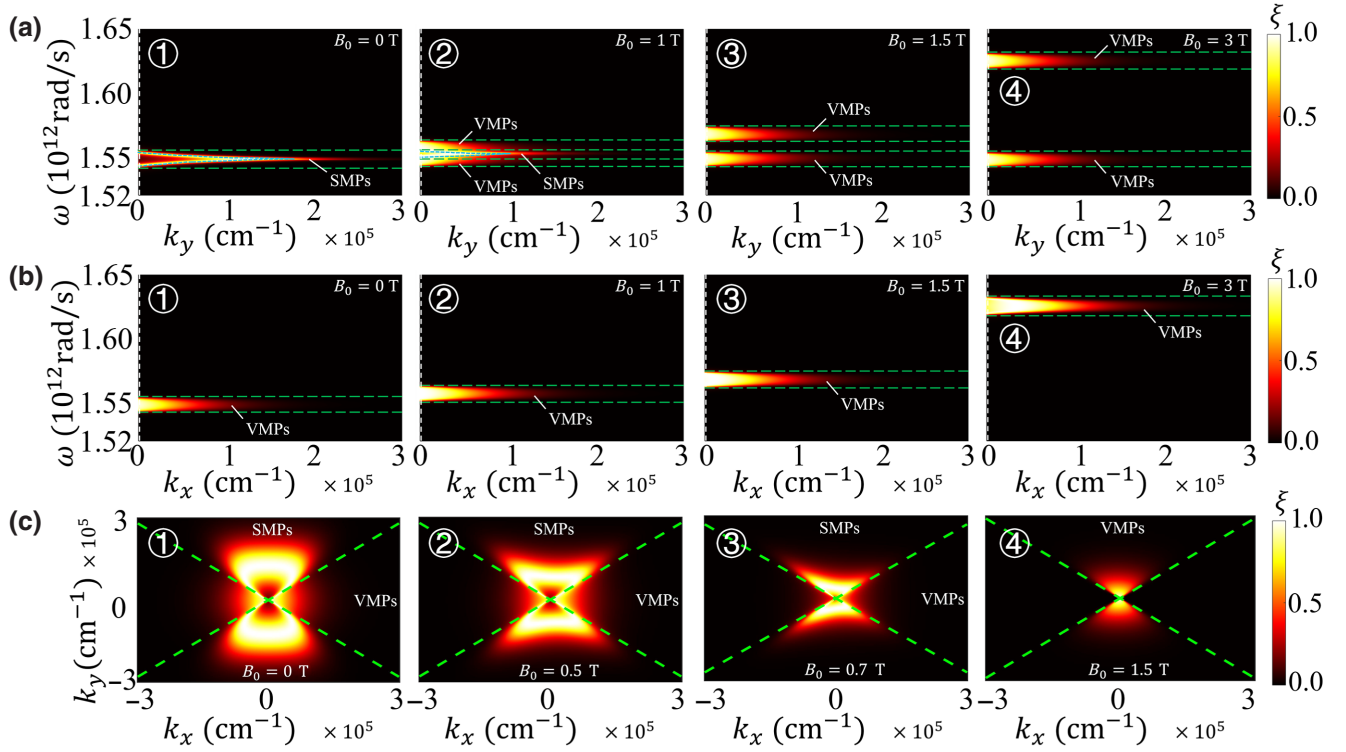
FIG. 3. (a) Energy transmission coefficients for the wave vector along the y direction ($k_x = 0$) for various magnetic fields. (b) Energy transmission coefficients for the wave vector along the x direction ($k_y = 0$) for various magnetic fields. The horizontal dashed lines separate the regions where transmission is dominated by surface waves or propagating waves. The cyan dashed lines correspond to the dispersion relation of the SMPs and the white dashed lines represent light cone in the vacuum. (c) Energy transmission coefficient with increasing twist angle at different magnetic fields. In (c), the frequency ω is fixed to 1.548×10^{12} rad/s and the green boundary lines for SMPs and VMPs are $k_y = \pm\sqrt{-\mu_{xx}/\mu_{yy}}k_x$. Note that in (a)–(c), twist angle $\theta = \pi$.

C. Field-induced topological transition of magnon polaritons

More magnetic effects of SMPs and VMPs can be presented in k_x-k_y space with fixed frequency. As shown in Fig. 3(c), SMPs and VMPs in k_x-k_y space are separated by the green boundary lines, i.e., $k_y = \pm\sqrt{-\mu_{xx}/\mu_{yy}}k_x$ with the biaxial approximation. At $B_0 = 0$ [Fig. 3(c)①], the whole system is reciprocal, and there is a coexistence of xy-symmetric elliptical SMPs and VMPs. With an increase in the magnetic field in the y direction, the time-reversal symmetry is broken, and the two types of modes gradually show nonreciprocity in the x direction. Next, we note that the topological structure of SMPs in k_x-k_y space can change from elliptical to hyperbolic with increasing magnetic field [Fig. 3(c)②,③]. Such a field-induced topological transition can reduce the contributions of SMPs in NFRHT. Moreover, we also find that there is a transition from type I VMPs to type II VMPs with increasing magnetic field, and there is only a type II VMP mode at a large magnetic field [Fig. 3(c)④]. Such field-induced transition effects can pave the way for more flexible thermal management at the nanoscale.

D. Dependence on θ of NFRHT and magnetic-field-reinforced thermal switch

We analyze the influence of twist angle θ on heat transfer in Fig. 4. At $B_0 = 0$ [Fig. 4(a)], there is coexistence of SMPs and VMPs separated by the above-mentioned boundary lines. With an increase in twist angle θ, we find that there is hybridization between SMPs and VMPs, and the boundary between the two modes can become trivial at $\theta = \pi/2$. Such twist-induced hybridization provides a convenient method for thermal management. Figures 4(b) and 4(c) show the cooperative effects of the magnetic field and twist angle θ. We find that two field-induced VMPs have completely different twist effects: low-frequency VMPs can be almost suppressed at $\theta = \pi/2$; in contrast, high-frequency VMPs only slightly change shape in k_x-k_y space. In addition, we notice that the high-frequency VMPs have a symmetric structure at $\theta = 0$ and remain nearly unchanged as the magnetic field increases because the whole system becomes symmetric again at $\theta = 0$. This effect corresponds to the purple dashed line in Fig. 2(a). These cooperative effects can construct a magnetic-field-reinforced thermal switch. We define the thermal switch
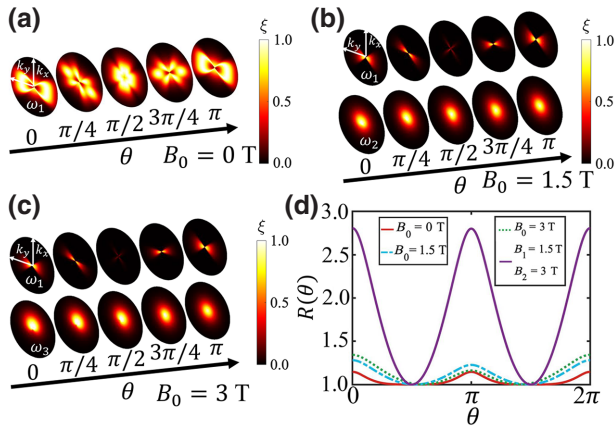
FIG. 4. (a) Energy transmission coefficients with twist angle increasing when $B_0 = 0$ T. (b) Energy transmission coefficients with twist angle increasing when $B_0 = 1.5$ T. (c) Energy transmission coefficients with twist angle increasing when $B_0 = 3$ T. (d) The thermal switch ratio as a function of twist angle with different magnetic field. Particularly, the purple curve corresponds to the case where applied magnetic fields on the two AFMI slabs are not equal. In (a)–(c), frequency $\omega_1 = 1.548 \times 10^{12}$ rad/s, $\omega_2 = 1.568 \times 10^{12}$ rad/s, and $\omega_3 = 1.625 \times 10^{12}$ rad/s.

ratio $R(\theta)$ as follows [27]:

$$R(\theta) = h(\theta)/h_{\min}. \qquad (8)$$

Figure 4(d) shows that the strength of the magnetic field can only enhance the thermal switch ratio in a relatively small range, i.e., from 1.1 at $B_1 = B_2 = 0$ T to 1.2 at $B_1 = B_2 = 1.5$ T or 1.25 at $B_1 = B_2 = 3$ T. However, the thermal switch ratio can be greatly boosted by the different configurations of applied magnetic fields: from 1.1 at $B_1 = B_2 = 0$ T to 2.8 at $B_1 = 1.5$ T, $B_2 = 3$ T. Combining all panels of Fig. 4, we can see that such a magnetic-field-reinforced thermal switch effect comes from the mismatch of high-frequency VMPs at different applied magnetic fields. From the viewpoint of symmetry analysis, we can find that this is a cooperative effect between rotational symmetry breaking and the external magnetic field (time-reversal symmetry breaking). Based on that, we can theoretically control the thermal switch ratio through an external magnetic field over a wide range.

IV. CONCLUSION

In summary, we show that the near-field radiative heat transfer between two hyperbolic antiferromagnet slabs can be controlled by external magnetic fields or twist angle θ between the two plates. Under time-reversal symmetry breaking, we find that the presence of a magnetic field makes the radiative heat flux change nonmonotonically irrespective of twist angle, and the minimum value can be found with fields of approximately 1.5 T. From the spectral function of the HTC, the heat flux contributed by SMPs is

gradually replaced by VMPs with increasing field. Then, SMPs can undergo a striking topological transition with increasing magnetic field, and similar types of VMPs can also change. Moreover, we find that twist-induced thermal switching is stronger with increasing field due to the nonzero off-diagonal element dependence of the nonreciprocity of VMPs. To realize an ultrastrong twist-induced thermal switch, we artificially choose the thermal transfer channel using different external magnetic fields, keeping the heat exchange channel sensitive to twist angle θ under configurational symmetry breaking. Finally, all the predictions of this work are amenable to measurements with present experimental techniques, and we are convinced that the multiple open questions that this work raises will motivate many further theoretical and experimental studies of this subject.

[1] S.-A. Biehs, M. Tschikin, R. Messina, and P. Ben-Abdallah, Super-planckian near-field thermal emission with phonon-polaritonic hyperbolic metamaterials, Appl. Phys. Lett. **102**, 131106 (2013).

[2] David G. Cahill, Paul V. Braun, Gang Chen, David R. Clarke, Shanhui Fan, Kenneth E. Goodson, Pawel Keblinski, William P. King, Gerald D. Mahan, Arun Majumdar, Humphrey J. Maris, Simon R. Phillpot, Eric Pop, and Li Shi, Nanoscale thermal transport. ii. 2003–2012, Appl. Phys. Rev. **1**, 011305 (2014).

[3] D. Polder and M. Van Hove, Theory of radiative heat transfer between closely spaced bodies, Phys. Rev. B **4**, 3303 (1971).

[4] A. I. Volokitin and B. N. J. Persson, Near-field radiative heat transfer and noncontact friction, Rev. Mod. Phys. **79**, 1291 (2007).

[5] G. A. Domoto, R. F. Boehm, and C. L. Tien, Experimental investigation of radiative transfer between metallic surfaces at cryogenic temperatures, J. Heat Transfer **92**, 412 (1970).

[6] J. B. Pendry, Radiative exchange of heat between nanostructures, J. Phys.: Condens. Matter **11**, 6621 (1999).

[7] W. A. Challener, Chubing Peng, A. V. Itagi, D. Karns, Wei Peng, Yingguo Peng, XiaoMin Yang, Xiaobin Zhu, N. J. Gokemeijer, Y.-T. Hsia, G. J.u Robert E Rottmayer, Michael A Seigler, and E. C. Gage, Heat-assisted magnetic recording by a near-field transducer with efficient optical energy transfer, Nat. Photonics **3**, 220 (2009).

[8] Barry C. Stipe, Timothy C. Strand, Chie C. Poon, Hamid Balamane, Thomas D. Boone, Jordan A. Katine, Jui-Lung Li, Vijay Rawat, Hiroaki Nemoto, Akemi Hirotsune, Olav Hellwig, Ricardo Ruiz, Elizabeth Dobisz, Dan S. Kercher,

Neil Robertson, Thomas R. Albrecht, and Bruce D. Terris, Magnetic recording at 1.5 pb m^{-2} using an integrated plasmonic antenna, Nat. Photonics **4**, 484 (2010).

[9] Rémi Carminati and Jean-Jacques Greffet, Near-Field Effects in Spatial Coherence of Thermal Sources, Phys. Rev. Lett. **82**, 1660 (1999).

[10] Jean-Jacques Greffet, Rémi Carminati, Karl Joulain, Jean-Philippe Mulet, Stéphane Mainguy, and Yong Chen, Coherent emission of light by thermal sources, Nature **416**, 61 (2002).

[11] Yannick De Wilde, Florian Formanek, Rémi Carminati, Boris Gralak, Paul-Arthur Lemoine, Karl Joulain, Jean-Philippe Mulet, Yong Chen, and Jean-Jacques Greffet, Thermal radiation scanning tunnelling microscopy, Nature **444**, 740 (2006).

[12] A. Kittel, U. F. Wischnath, J. Welker, O. Huth, F. Rüting, and S.-A. Biehs, Near-field thermal imaging of nanostructured surfaces, Appl. Phys. Lett. **93**, 193109 (2008).

[13] Andrew C. Jones, Brian T. O'Callahan, Honghua U. Yang, and Markus B. Raschke, The thermal near-field: Coherence, spectroscopy, heat-transfer, and optical forces, Prog. Surf. Sci. **88**, 349 (2013).

[14] P. J. van Zwol, S. Thiele, C. Berger, W. A. de Heer, and J. Chevrier, Nanoscale Radiative Heat Flow due to Surface Plasmons in Graphene and Doped Silicon, Phys. Rev. Lett. **109**, 264301 (2012).

[15] Clayton R. Otey, Wah Tung Lau, and Shanhui Fan, Thermal Rectification Through Vacuum, Phys. Rev. Lett. **104**, 154301 (2010).

[16] Philippe Ben-Abdallah and Svend-Age Biehs, Near-Field Thermal Transistor, Phys. Rev. Lett. **112**, 044301 (2014).

[17] Riccardo Messina and Philippe Ben-Abdallah, Graphene-based photovoltaic cells for near-field thermal energy conversion, Sci. Rep. **3**, 1383 (2013).

[18] K. Park, S. Basu, W. P. King, and Z. M. Zhang, Performance analysis of near-field thermophotovoltaic devices considering absorption distribution, J. Quant. Spectrosc. Radiat. Transfer **109**, 305 (2008).

[19] Jared W. Schwede, Igor Bargatin, Daniel C. Riley, Brian E. Hardin, Samuel J. Rosenthal, Yun Sun, Felix Schmitt, Piero Pianetta, Roger T. Howe, Zhi-Xun Shen, and Nicholas A. Melosh, Photon-enhanced thermionic emission for solar concentrator systems, Nat. Mater. **9**, 762 (2010).

[20] Jean Philippe Mulet, Karl Joulain, Rémi Carminati, and Jean Jacques Greffet, Enhanced radiative heat transfer at nanometric distances, Microscale Thermophys. Eng. **6**, 209 (2002).

[21] Hideo Iizuka and Shanhui Fan, Analytical treatment of near-field electromagnetic heat transfer at the nanoscale, Phys. Rev. B **92**, 144307 (2015).

[22] Jiawei Shi, Pengfei Li, Baoan Liu, and Sheng Shen, Tuning near field radiation by doped silicon, Appl. Phys. Lett. **102**, 183114 (2013).

[23] Mikyung Lim, Seung S. Lee, and Bong Jae Lee, Near-field thermal radiation between doped silicon plates at nanoscale gaps, Phys. Rev. B **91**, 195136 (2015).

[24] Victor W. Brar, Min Seok Jang, Michelle Sherrott, Seyoon Kim, Josue J. Lopez, Laura B. Kim, Mansoo Choi, and Harry Atwater, Hybrid surface-phonon-plasmon polariton modes in graphene/monolayer h-BN heterostructures, Nano Lett. **14**, 3876 (2014).

[25] Anshuman Kumar, Tony Low, Kin Hung Fung, Phaedon Avouris, and Nicholas X. Fang, Tunable light–matter interaction and the role of hyperbolicity in graphene–hBN system, Nano Lett. **15**, 3172 (2015).

[26] S. Dai, Q. Ma, M. K. Liu, T. Andersen, Z. Fei, M. D. Goldflam, M. Wagner, K. Watanabe, T. Taniguchi, M. Thiemens, F. Keilmann, G. C. A. M. Janssen, S.-E. Zhu, P. Jarillo-Herrero, M. M. Fogler, and D. N. Basov, Graphene on hexagonal boron nitride as a tunable hyperbolic metamaterial, Nat. Nanotechnol. **10**, 682 (2015).

[27] Jiebin Peng, Gaomin Tang, Luqin Wang, Rair Macêdo, Hong Chen, and Jie Ren, Twist-induced near-field thermal switch using nonreciprocal surface magnon-polaritons, ACS Photonics **8**, 2183 (2021).

[28] Rair Macêdo and Robert E. Camley, Engineering terahertz surface magnon-polaritons in hyperbolic antiferromagnets, Phys. Rev. B **99**, 014437 (2019).

[29] P. J. van Zwol, K. Joulain, P. Ben Abdallah, J. J. Greffet, and J. Chevrier, Fast nanoscale heat-flux modulation with phase-change materials, Phys. Rev. B **83**, 201404(R) (2011).

[30] Yi Huang, Svetlana V. Boriskina, and Gang Chen, Electrically tunable near-field radiative heat transfer via ferroelectric materials, Appl. Phys. Lett. **105**, 244102 (2014).

[31] E. Moncada-Villa, V. Fernández-Hurtado, F. J. García-Vidal, A. García-Martín, and J. C. Cuevas, Magnetic field control of near-field radiative heat transfer and the realization of highly tunable hyperbolic thermal emitters, Phys. Rev. B **92**, 125418 (2015).

[32] Ivan Latella and Philippe Ben-Abdallah, Giant Thermal Magnetoresistance in Plasmonic Structures, Phys. Rev. Lett. **118**, 173902 (2017).

[33] Gaomin Tang, Jun Chen, and Lei Zhang, Twist-induced control of near-field heat radiation between magnetic Weyl semimetals, ACS Photonics **8**, 443 (2021).

[34] Cheng Guo, Bo Zhao, Danhong Huang, and Shanhui Fan, Radiative thermal router based on tunable magnetic Weyl semimetals, ACS Photonics **7**, 3257 (2020).

[35] Bo Zhao, Cheng Guo, Christina A. C. Garcia, Prineha Narang, and Shanhui Fan, Axion-field-enabled nonreciprocal thermal radiation in Weyl semimetals, Nano Lett. **20**, 1923 (2020).

[36] S.-A. Biehs, F. S. S. Rosa, and P. Ben-Abdallah, Modulation of near-field heat transfer between two gratings, Appl. Phys. Lett. **98**, 243102 (2011).

[37] Ming-Jian He, Hong Qi, Ya-Tao Ren, Yi-Jun Zhao, Yong Zhang, Jia-Dong Shen, and Mauro Antezza, Radiative thermal switch driven by anisotropic black phosphorus plasmons, Opt. Express **28**, 26922 (2020).

[38] Yuan Cao, Valla Fatemi, Shiang Fang, Kenji Watanabe, Takashi Taniguchi, Efthimios Kaxiras, and Pablo Jarillo-Herrero, Unconventional superconductivity in magic-angle graphene superlattices, Nature **556**, 43 (2018).

[39] Yuan Cao, Debanjan Chowdhury, Daniel Rodan-Legrain, Oriol Rubies-Bigorda, Kenji Watanabe, Takashi Taniguchi, T. Senthil, and Pablo Jarillo-Herrero, Strange Metal in Magic-Angle Graphene with Near Planckian Dissipation, Phys. Rev. Lett. **124**, 076801 (2020).

[40] S. S. Sunku, G. X. Ni, B. Y. Jiang, H. Yoo, A. Sternbach, A. S. McLeod, T. Stauber, L. Xiong, T. Taniguchi, K. Watanabe, P. Kim, M. M. Fogler, and D. N. Basov, Photonic crystals for nano-light in moiré graphene superlattices, Science **362**, 1153 (2018).

[41] Guangwei Hu, Alex Krasnok, Yarden Mazor, Cheng-Wei Qiu, and Andrea Alù, Moiré hyperbolic metasurfaces, Nano Lett. **20**, 3217 (2020).

[42] N. S. Almeida and D. L. Mills, Dynamical response of antiferromagnets in an oblique magnetic field: Application to surface magnons, Phys. Rev. B **37**, 3400 (1988).

[43] Fred M. Johnson and Arthur H. Nethercot, Antiferromagnetic resonance in MnF_2, Phys. Rev. **114**, 705 (1959).

[44] Rair Macêdo, Thomas Dumelow, and Robert L. Stamps, Tunable focusing in natural hyperbolic magnetic media, ACS Photonics **3**, 1670 (2016).

[45] L. Remer, B. Lüthi, H. Sauer, R. Geick, and R. E. Camley, Nonreciprocal Optical Reflection of the Uniaxial Antiferromagnet MnF_2, Phys. Rev. Lett. **56**, 2752 (1986).

[46] Simo Pajovic, Yoichiro Tsurimaki, Xin Qian, and Svetlana V. Boriskina, Radiative heat and momentum transfer from materials with broken symmetries: Opinion, Opt. Mater. Express **11**, 3125 (2021).